MTI Core Science Retrieval Algorithms

Christoph C. Borel, William B. Clodius, Anthony B. Davis, Barham W. Smith,
John J. Szymanski, James Theiler, Pierre V. Villeneuve and Paul G. Weber
Space and Remote Sensing Sciences Group
Mailstop C 323, Los Alamos National Laboratory
Los Alamos, NM 87545, USA
cborel@lanl.gov

ABSTRACT

The Multispectral Thermal Imager (MTI) has a number of core science retrievals which will be described. We will concentrate on describing the major Level-2 algorithms which cover land, water and atmospheric products. The land products comprise atmospherically corrected surface reflectances, vegetation health status, material identification, land temperature and emissivities. The water related products are: water mask, water quality and water temperature. The atmospheric products are: cloud mask, cirrus mask and atmospheric water vapor. We will present several of these algorithms and present results from simulated MTI data derived from AVIRIS and MODIS Airborne Simulator (MAS). An interactive analysis tool has been created to visually program and test certain Level-2 retrievals.

1. Introduction and overall organization

MTI is both a technology demonstration as well as a mission to apply science-based retrieval algorithms to problems of interest to the Department of Energy. We have been tasked to develop analysis methods to monitor cooperative industrial facilities and other environmental applications. A list of the bands and applications of MTI is shown in Table 1.

Retrievals with direct applications to monitoring industrial activity at cooperating sites are depicted in Figure 1. We perform atmospheric correction of the measured radiances to ground reflectances (Borel et al, 1999a), unmixing of mixed land/water pixels (Szymanski et al, 1999) and water depth (bathymetry) and material identification. Previous work on adjacency effect corrections (Borel and Gerstl, 1992) will be applied for special cases where hazy conditions cause scattering of photons from outside the line of sight surfaces into the imager.

Band Characteristics				Use in Science Analysis (D=Day, N=Night)						
Band	Wavelength in μm	Color/ Region	Major Appl.	Sea Surf. Temp.	Water Qual.	Water Vapor	Atm. Corr.	Veg. Stress	Cirrus Detect.	Class./ Mat .Id.
A	0.45-0.52	blue/grn.	Water		D		D			D
B	0.52-0.60	grn/yel.	Soil/Veg.		D		D	D		D
C	0.62-0.68	red	Chloroph.		D		D	D		D
D	0.76-0.86	NIR	Veg.	(D)			D	D		D
E	0.86-0.90	NIR	H_2O Ref.	(D)		D	D			
F	0.91-0.97	NIR	H_2O Abs.	(D)		D	D			
G	0.99-1.04	SWIR	H_2O Ref.			D	D			D
H	1.36-1.39	SWIR	Cirrus				D		D	
I	1.55-1.75	SWIR	Veg.				D	D		D
O	2.08-2.35	SWIR	Geology				D	D		D
J	3.50-4.10	MWIR	Therm.	N						D+N
K	4.87-5.07	MWIR	Therm.	D+N				D		N
L	8.00-8.4	LWIR	Therm.	D+N				D		N
M	8.40-8.85	LWIR	Therm.	D+N				D		N
N	10.15-11.5	LWIR	Therm.	D+N				D		N

Table 1. MTI's bands and their day (D) and night (N) time applications, in brackets are channels which contribute.

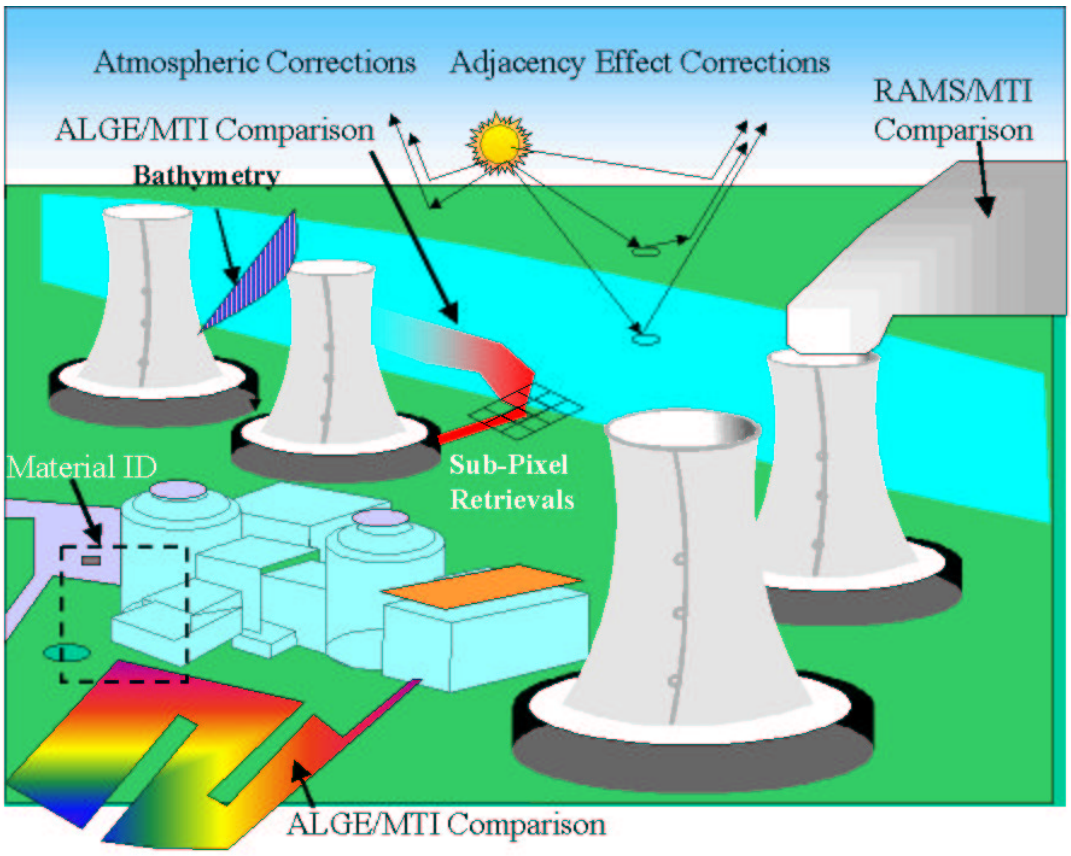

Figure 1. MTI's industrial facilities monitoring products.

Level-2 products will be input to Level-4 products in models such as ALGE (a 3-d hydrodynamics code to simulate thermal transport in rivers, cooling ponds and estuaries). A special version of the Regional Atmospheric Modeling System (RAMS) will model cooling tower plumes (see Garrett et al, 1999) using input from water vapor retrievals and plume temperature. We will compare retrieved quantities to ground truth from our cooperative sites. Environmental applications are of interest as well and applications are depicted in Figure 2. There are many waste sites located on DOE and other government sites which need to be monitored periodically to estimate changes in crop status, vegetation health, air and water quality. Not yet well defined are SO_2 gas detection in volcanic plumes and water vapor mapping for evapotranspiration studies.

There is a large effort underway within NASA to study the Earth on a global scale. MTI offers a high-spatial resolution view of certain sites at a different time of over-flight than that of the EOS-AM platform. MTI's ability to take near-simultaneous 2-look images in the thermal will be important for understanding angular brightness and reflectance variations of other sensors such as ISR, MODIS and ASTER.

Figure 3 shows a diagram to show the data flow from calibrated radiances to the various Level-2 products. The various products are tightly coupled, e.g. to determine water temperature we need to identify water using a water mask and screen for cirrus and other clouds. This can only be done after top of the atmosphere (TOA) radiances have been converted to ground reflectances. That in turn requires calculation of atmospheric parameters such as aerosol optical thickness and columnar water vapor amount.

2. Land Products

MTI is a very well calibrated multi-spectral sensor and as such should be able to retrieve good absolute reflectance measurements over land surfaces. Absolute or normalized (to eliminate illumination effects) reflectances can then be used to identify different materials.

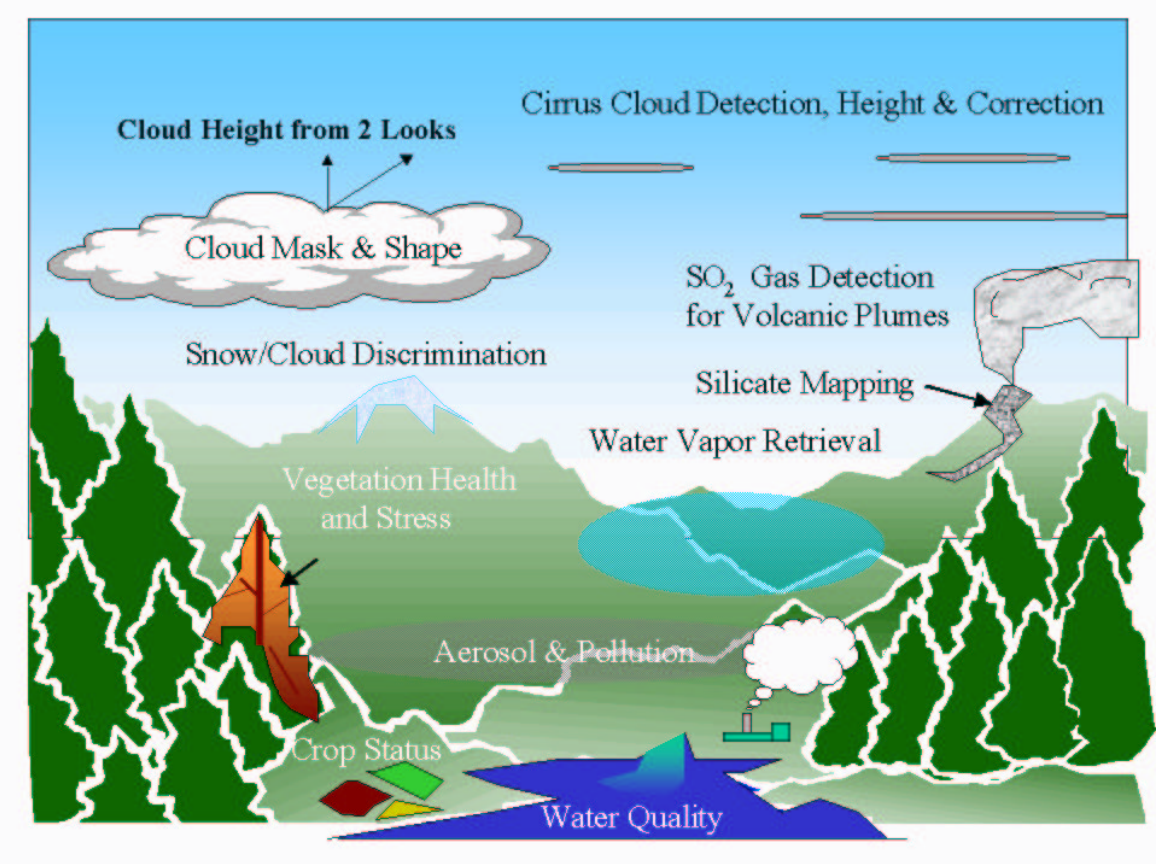

Figure 2. MTI's environmental science products.

2.1. Surface reflectance retrieval

Our approaches to atmospheric corrections have been detailed in a previous paper (Borel et al, 1999a) and will be summarized here. Typically available atmospheric correction methods, are based on detailed radiative transfer models, such as MODTRAN and 6S. These codes require the specification of usually unknown atmospheric parameters such as aerosol optical depth and water vapor amount for which MTI has special spectral channels to retrieve them. We have developed two practical atmospheric correction methods which use scene radiances directly to correct for the atmosphere.

2.1.1. Dense dark vegetation based atmospheric correction

The first in-scene atmospheric correction method is based on a retrieval of aerosol optical depth over dense dark vegetative canopies. Due to the fact that the A and B absorption bands of chlorophyll leaves reflect very little (2-5%) in the red (channel C) and somewhat more (8-12%) in channel B. Kaufman et al., 1996, have found a strong correlation between dense dark vegetation reflectances ρ_O and ρ_B as well as ρ_O and ρ_C. We computed this correlation using the N-layer canopy radiosity model described in Borel and Gerstl, 1992 and the PROSPECT leaf model by Jacquemoud (1995). The canopy had uniformly distributed random Leaf Area Indices (LAI's) between 4 and 8, a random mixture of soils as a background and green leaves (chlorophyll content between 25 and 34 $\mu g/cm^2$). The computed reflectance ratio ρ_B/ρ_O is about unity and 1/4 for ρ_C/ρ_O which is close to the reported values by Kaufman et al, 1996. Using dark vegetative canopies and the correlation relationship, it is possible to determine the aerosol optical loading using a look-up-table as described in Borel et al, 1999a.

2.1.2. Water based atmospheric correction

The second in-scene atmospheric correction method is based on path reflectance estimates over water surfaces in the near infrared (NIR) and short wave infrared (SWIR). It was observed (Borel et al, 1999a) that for atmospheric

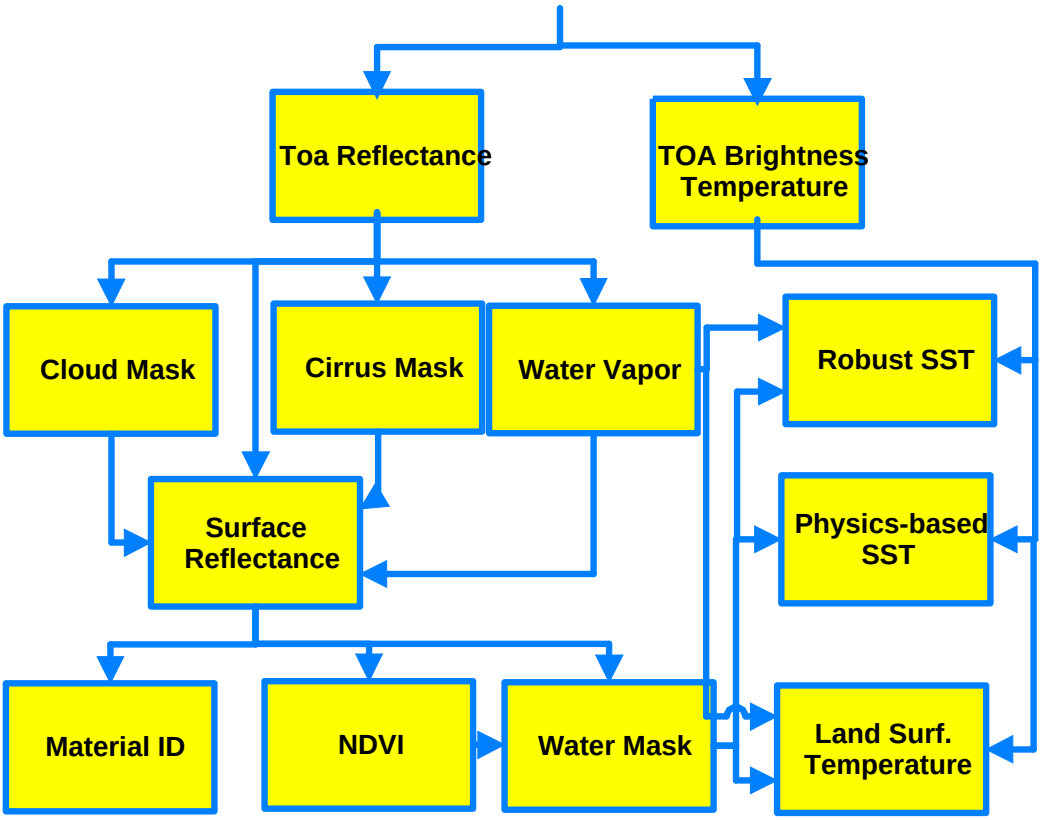

Figure 3. MTI's industrial facilities and environmental Level-2 science product flow.

windows (all VIS/SWIR channels except H) the logarithm of the band integrated path reflectance is a almost linear function of the logarithm of the center wavelengths:

$$\rho^*_{i;corrected} = \rho^*_{i;TOA} - \rho_{i;path}, \quad \text{where} \rho_{i;path} = 10.^{a+b\ \log_{10}(\lambda_i)}. \tag{1}$$

In this method we neglect the absorption through the atmosphere and local illumination geometry. We plan on building in a correction for the atmospheric transmission losses and illumination geometry.

2.2. Vegetation health status retrieval

Vegetation health has different signatures depending on its stress factors. In this section we do not distinguish between antropogenic and natural plant stress factors but note that they are often difficult to distinguish. The simplest vegetation condition retrieval is the $NDVI$ which is related to the leaf area index has been implemented as well as three channels indices related to chlorophyll. Both require surface reflectance data. The following description of various vegetation stress types and their signatures will be useful in generating MTI algorithms for vegetation stress:

1. Water Stress:

   (a) Leaf water signature: Water stress for example may be measured using the 940 nm water absorption region using 3 or more channels. MTI may be able to retrieve a rough estimate using 3 channel water vapor retrieval method when there are bare soil areas near vegetative canopies for a uniformly mixed boundary layer. The soil should not have other absorption features for leaf water retrievals to work, i.e. should not contain iron oxide or gypsum. In Borel et al, 1996b we list many materials which would produce water vapor retrieval errors. For the case when the true atmospheric water vapor can be obtained over the bare soil the difference to water vapor retrieved nearby vegetative canopies is proportional to the total canopy water content which of course also depends on the LAI. The effect of changing water vapor ratios with LAI has been modeled in Borel et al, 1996b.

(b) Temperature: In certain plants water stress also increases the apparent leaf temperature since the leaf stomata stop evaporating water to conserve water.

(c) Canopy angular reflectance: Water stress can change the canopy architecture and thus change the bi-directional reflectance which is largely proportional to the percentage of illuminated versus shaded phyto-elements (leaves, branches). As water stress increases, some plants re-orient their leaves to intercept less light, thus the percentage of illuminated visible leaves goes down for most view angles. In an experiment performed in 1990 the author stressed cotton plants by cutting off their water supply and found an overall decrease in the angular reflectance of 10 % in the visible and NIR within 15 minutes of the cutting. Given two look-angles for MTI we may be able to detect changes in the leaf angle distribution.

2. Nutrient stress:

(a) Leaf spectral signature: Nutrient stress often is indicated by yellowed leaves due to a smaller than normal amount of chlorophyll in leaves. Thus a three channel detection scheme using the area of a triangle formed by the reflectances of the green, red and NIR channels in a spectral plot is be able to detect such stressed plants, e.g. Borel, 1996a.

(b) Canopy spectral signature: Lack of nutrients manifests itself often in smaller and fewer leaves thus in less dense canopies. A good measure is the Leaf Area Index (LAI) which is often obtained by ratios of red and NIR channels. We have investigated 8 different vegetation indices for a large number of simulated canopies, Borel, 1996a. We found that neural nets can be used not only to derive the LAI but also the nitrogen content and fractions of soil constituents under low-LAI canopies ($LAI < 1$), Gisler and Borel, 1996.

2.3. Material identification

The purpose of this algorithm is to identify specific materials within an MTI scene. An important aspect of material identification is distinguishing man-made objects from natural objects. Most man-made objects are made of metals, plastics, concrete, etc. that have distinctive spectral signatures when compared to naturally occurring materials. We currently have 4 tools to help with material identification.

2.3.1. Un-supervised k-means clustering

In an un-supervised algorithm, we identify materials from multispectral imagery using the k-means clustering algorithm. A more advanced algorithm we have available is the contiguity enhanced k-means clustering algorithm, Theiler and Gisler, 1997. Most k-means clustering algorithm involve an iterative scheme which operates over a fixed number of clusters, while attempting to satisfy the following conditions: (1) Each cluster has a center which is the mean position of all samples in that cluster. (2) Each sample is a member of the cluster to whose center it is closest. The clustering process is started with an initial clustering of the data (which may be random), and then passes from sample to sample, assigning each to the nearest cluster. The cluster centers are recomputed after each data sample reassignment. The total number of clusters is not automatically calculated by the algorithm and must be specified by the user. To make the program run faster we select a random subset of pixels in the scene (typically 1000-9000). The user has to assign class types later to each cluster.

2.3.2. Spectral angular mapper material identification

Often we can identify a building or other object in the scene and would like to identify other areas with similar spectral signatures. A very simple algorithm is the Spectral Angle Mapper (SAM) which was introduced to remote sensing by Boardman in 1993 (unpublished work cited in Kruse et al, 1993). At pixel (i, j) SAM computes the angle $\alpha_{i,j}$ between a reference spectrum $\vec{r}$ and a measured spectral data cube $\vec{t}_{i,j}$. The angle is the inverse cosine of the "dot" product of the normalized spectral vector $\vec{r}/|\vec{r}|$ and the normalized vector $\vec{t}_{i,j}/|\vec{t}_{i,j}|$. The SAM can be written as sums over all N spectral channels:

$$\alpha_{i,j} = \cos^{-1}\left(\frac{\sum_{n=1}^{N} r_n t_{n;i,j}}{\sqrt{\sum_{n=1}^{N} r_n^2}\sqrt{\sum_{n=1}^{N} t_{n;i,j}^2}}\right) \tag{2}$$

The SAM is insensitive to the illumination conditions. In our implementation a pixel r is selected interactively and then a cumulative histogram over α is displayed in a log-lin plot allowing the user to select a threshold angle α_{thres} for which to display a normalized image of $\alpha_{i,j} < \alpha_{thres}$.

2.3.3. Spectral library based material identification

Four spectral libraries with a total of approximately five hundred spectra were used in the creation of our spectral database. These spectra were obtained in part from the NIST (http://ciks.cbt.nist.gov/nef/), Salisbury and the JPL spectral libraries (http://speclib.jpl.nasa.gov/). The user can select any spectrum and calculate the Mean Square Error (MSE) between measured reflectance $\vec{t}_{i,j}$ and k-th material spectrum $\vec{r}_k$. The user selects then one of the close matches based on visual agreements and some additional knowledge about the scene.

2.3.4. Supervised land cover classification

Some users of MTI will be interested in generating land cover classification for environmental applications and temporal studies. Currently we use a land cover classification system from USGS, e.g. Jensen, 1996, which divides land covers into nine classes each with several sub-classes. We added a class called "Others" to be able to add clouds and cloud shadow. The user selects a given sub-class and then marks a region using a polygon in the image. All spectra in the region are extracted and mean and standard deviation are computed.

3. Water products

Many important MTI retrievals concern water. The initial steps in our analysis determine a water mask at 5 m GSD, which is then used to mask more complex products such as surface reflectance, water quality and water temperature.

3.1. Water mask retrieval

Water masks can be obtained using three methods using only the first four channels(A, B, C and D) of MTI which have a smaller Ground Sample Distance (GSD) then the others. Besides the methods described below we have a team working on genetic algorithms and one of their applications was to try to find a water mask, Brumby et al, 1999.

3.1.1. NDVI and reflectance based water mask

The simplest water mask was described in Borel et al, 1999a. It uses a logical "and" of a threshold in the red channel TOA reflectance ρ_C and a threshold on the Normalized Difference Vegetation Index ($NDVI$) computed from the TOA reflectances of channels C and D:

$$WM_{simple} = (\rho_C < 0.3) \cap (NDVI < 0.041), \tag{3}$$

where $NDVI = (\rho_D - \rho_C)/(\rho_D + \rho_C)$.

3.1.2. Spectral water mask

Two more sophisticated water masks have been devised using trial and error and logical operations between various functions of the TOA channel reflectances. Note we use TOA reflectances since the water masks themselves are later used for the computation of the surface reflectances. The "spectral water mask" has the form:

$$WM_{spectral} = (norm(\rho_D) \leq 0.25) \cap (NDVI \leq 0.) \cap (\rho_B/\rho_C > 1.), \tag{4}$$

where $norm(\rho_i)$ is computed by normalizing the channel i TOA reflectance between 0.0 and 1.0 so that 96% of the data lies in that interval.

3.1.3. Spatial water mask

The "spatial water mask" makes use of the fact that the standard deviation of regions within a body of water is usually much smaller than that of land and that for sub-pixel size streams and on the periphery of water bodies pixels are mixed:

$$WM_{spatial} = (WM_1 + WM_2 + WM_3) \geq 2, \tag{5}$$

where

$$\begin{aligned} WM_1 &= (norm(\rho_D) \leq 0.25) \cap (NDVI \leq 0.), \\ WM_2 &= (NDVI > 0.) \cap (norm(\sigma(\rho_D)) \leq 0.25), \text{ and} \\ WM_3 &= (norm(\rho_D) \leq 0.25) \cap (HP(\rho_D) > 0.) \cap (norm(\sigma(\rho_D)) \geq 0.25). \end{aligned} \tag{6}$$

The notation $\sigma(\rho_i)$ is the standard deviation of channel TOA reflectance i computed for each pixel using a sliding window with size n by n pixels. The notation $HP(\rho_i)$ is the high-pass filtered image of channel TOA reflectance i computed by the difference between a pixel and the average over a n x n window centered around the pixel. Condition WM_3 is useful since it adds an extra pixel around the boundary of water bodies and brings out small sub-pixel streams. We found $n = 11$ to work for scenes from the MODIS Airborne Simulator (MAS). Note, we did not eliminate repeated logical statements in eq. (6) to leave open the option of applying different thresholds, e.g. for $NDVI$.

3.2. Water quality retrieval

Water quality near sea shores, rivers and ponds depends on the amount and proportions of chlorophyll-a, sediments and yellow substance (colored dissolved organic matter (CDOM), gelbstoff, detritus). The chlorophyll determines the amount of living organisms near the surface. The presence of suspended sediments and yellow substance (and the lack of them) are important in analyzing discharges into a river.

In a cooling pond the retrieval of the amount of chlorophyll in water is an indicator of the water temperature. It has been shown that there is a relation between chlorophyll content and water temperature. Thus chlorophyll retrieval in an indirect way will help determine the water temperature.

We are using the atmospheric transfer code 6S (Vermote, 1997) to compute top of the atmosphere radiance and apparent reflectance in MTI channels A, B, C and D. A BRDF model of a water surface is included in the code with the following features:

- Specular reflection from water is modeled using Fresnel reflection.
- Surface slope distribution as a function of wind speed using the Cox-Munk model for solar glint.
- White-cap contributions for high wind velocities are included.
- Chlorophyll concentration effects on water color are modeled using Morel's (1988) model.

The current algorithm consists of the following steps:

1. Generate input file for 6S for given observation.
2. Run IDL wrapper program to generate top of the atmosphere radiances for channels A, B and C.
3. Run polynomial fitting program to fit the chlorophyll content as a function of channel radiance ratios A/B and B/C.

In Figure 4 we show how the ratio of radiances from channels B/A and C/B relate to chlorophyll concentration. The Cox-Munk parameter for a wind speed was set to 2 m/s. The visibility was 23 km with a sun angle at 45 degrees and nadir observation. Notice the difficulty to measure chlorophyll concentration in the open ocean (left plot) above some minimum concentration. However it should be easier for in-land waters as shown in the right plot.

3.3. Sea surface temperature retrieval

We have implemented two different methods to estimate the sea surface temperature (SST). On is based on a statistical approach and the other based on physical principals. Both approaches can with some modifications and limitations be used to retrieve land surface temperatures as well.

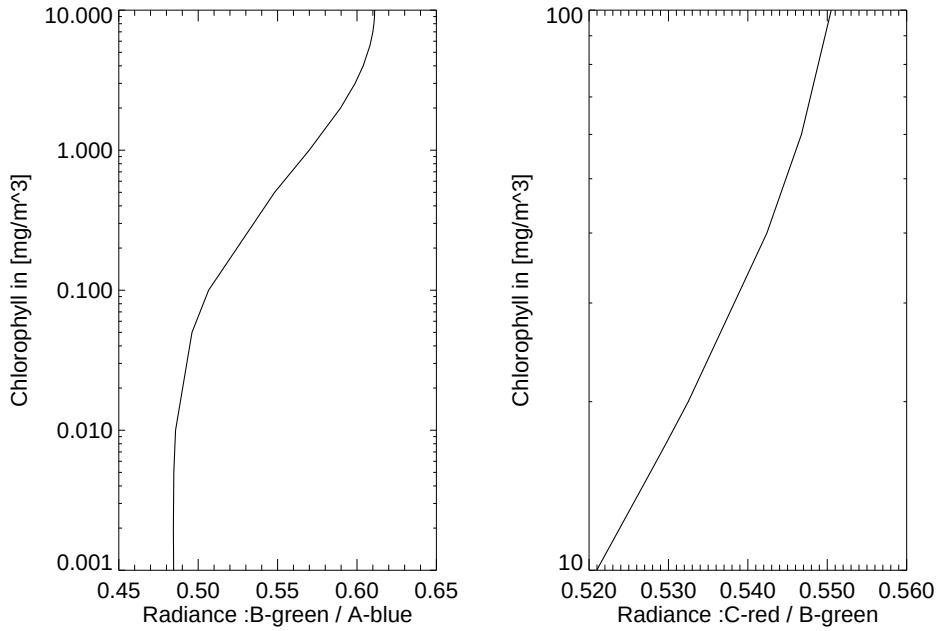

Figure 4. TOA Radiance ratios to retrieve chlorophyll content for ocean (left) and in-land waters (right).

3.3.1. Robust sea surface temperature retrieval

The first we call "robust" since it does not require detailed knowledge of the atmosphere. The SST accuracy can be improved by specifying some general condition like dry, medium wet and wet. Details can be found in Tornow et al, 1994a+b. The robust SST is based on two looks of the body of water at nadir and 60^o. The algorithm we developed is based on linear combinations of the brightness temperatures in channels J ,K ,L ,N and M (10 measurements) during night time and four channels (K, L, M and N) (8 measurements) during the daytime. Adding a term proportional to the columnar water vapor improves the SST accuracy during the day. The flow diagram on how to obtain the regression coefficients is shown in Figure 5. The intermediate radiance database contains information on atmospheric transmission, up-welling radiance, and reflected down-welling radiance for a wide range of atmospheric conditions, as seen in the five thermal bands at two different look-angles. Generating the intermediate database involves a large number of MODTRAN runs. From these intermediate values, the final TOA radiance for a given water emissivity and and water temperature can be quickly computed (without recourse to MODTRAN). An extended radiance database can then be built with TOA radiances (or, equivalently, TOA brightness temperatures) in each of the ten band/angle combinations over a wide range of water temperatures. Using linear regression, coefficients are found which optimally fit the water temperature as a function of TOA brightness temperatures. These coefficients comprise the robust SST retrieval algorithm.

3.3.2. Physics-based SST retrieval

Two related variations of a physics-based SST algorithm were developed to check the consistency of the robust SST retrievals. The algorithm is described in more detail in Borel et al, 1999b. The main idea is that for a single pixel atmospherically-corrected SST temperature should be the same in all thermal channels. The measured radiance $L_{m,i}$ for channel i at an observation angle of θ can be modeled as:

$$L_{m,i} = \varepsilon_{w,i} B_i(T_w)\tau_i(CW,\theta) + B_i(T_a)[1-\tau_i(CW,\theta)] \tag{7}$$

where ε_w is the water emissivity, $B_i(T)$ is the band-averaged Planck function for band i with the subscripts w indicating water and a indicating the atmosphere. The columnar water vapor dependent transmission is written

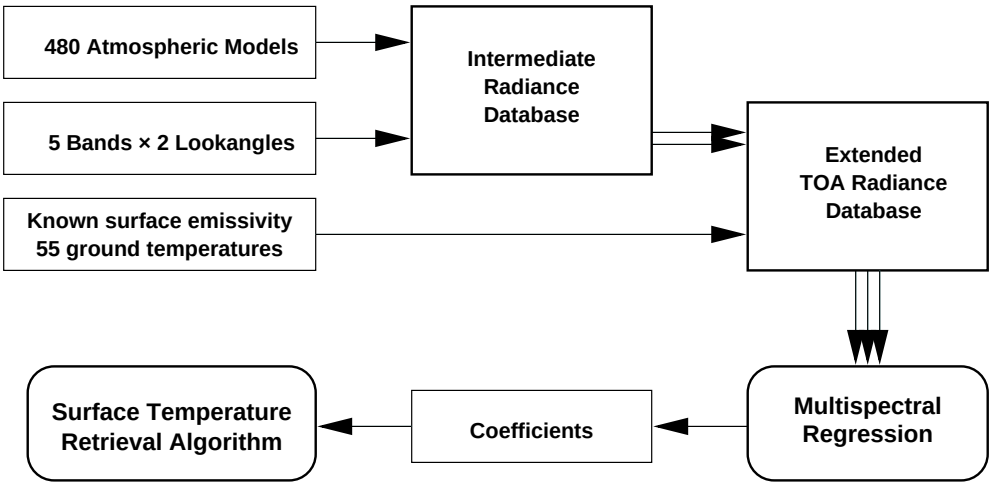

Figure 5. Flow diagram for the determination of the band coefficients for the robust SST retrieval.

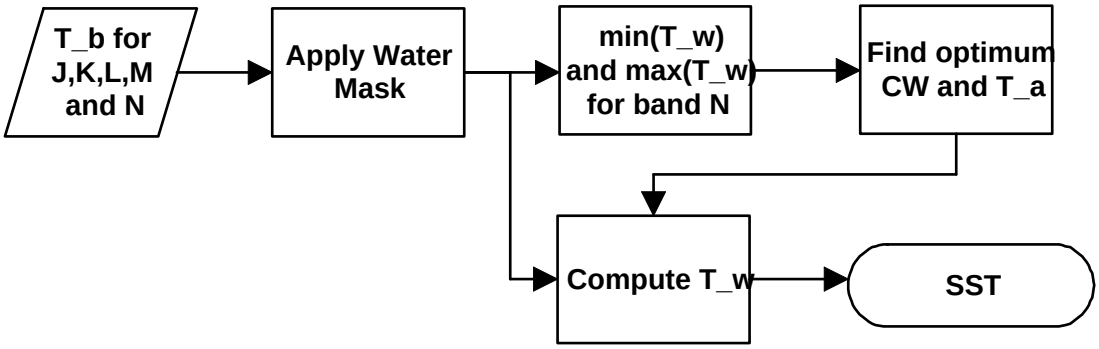

Figure 6. Flow diagram for physics-based multi-pixel SST retrieval.

as $\tau_i(CW, \theta)$ and can be approximated by:

$$\tau_i(CW, \theta) = \exp[-(\frac{A_i}{\cos\theta} + B_i(\frac{CW}{\cos\theta})^{C_i})] \tag{8}$$

where A_i, B_i and C_i are fitting parameters obtained by varying the columnar water vapor for nadir looks. Equations (7) and (8) form a nonlinear system of 5 (4 at night) equations where the unknowns T_w, T_a and CW are independent of wavelength. There are many solutions possible of T_a and CW which minimize the standard deviation σ over the retrieved water temperatures. However the error between retrieved water temperature $\hat{T_w}$and actual water temperature is negligible.

If water surfaces are at different temperatures, e.g. a river and a lake or a natural lake and a cooling pond, we found that a unique set of T_a and CW can be found by combining the error surfaces for the minimum and maximum water temperatures. A flow diagram of the multi-pixel SST retrieval is shown in Figure 6.

4. Atmospheric products

Scenes often contain clouds which can significantly impact atmospheric correction results when ignored and thus must be detected, masked out and in the case of thin cirrus corrected. Material identification in the cloud shadow will have to be based on normalized spectra rather than surface reflectances. Clouds also need to be screened before further analysis steps such as principal components are applied. For example if cloud pixels were included in the analysis, they would dominate the variability of the principal components from those obtained to a cloud-free scene.

4.1. Cloud and cloud shadow mask retrieval

The lack of direct illumination in cloud shadows prevents present atmospheric correction algorithms from retrieving reflectances and thus should be detected. In an earlier paper (Borel et al, 1999a) we showed a simple algorithm for generating a cloud mask using the $NDVI$ (which is close to zero for clouds) and a reflectance threshold in the red where many surfaces are dark. skew the principal components. The following simple algorithm produced a mask for the cloud shadow (CS) using 9 simulated MTI channel data (all channels except H):

$$CS = R_9 < 1.82/min(R_9)] \cap not(WM), \text{ where } \mathrm{R_9} = \frac{1}{9}\sqrt{\sum_{\mathrm{i}=1}^{9} \rho_{\mathrm{i}}^2}. \tag{9}$$

The variable WM is a water mask. Water needs to be excluded from the cloud shadow mask. Of course if the cloud shadow falls on water, then it cannot be detected and the water mask should not be used in eq. (9).

4.2. Correcting for cirrus clouds

A simple interactive algorithm was developed to correct for thin cirrus in MTI's bands. The data used was taken by AVIRIS over Coffeyville, Kansas on December 1, 1991. After converting it to band averaged TOA reflectances, we manually chose regression coefficients a_i and b_i on a scatter plot with axes: $x = \rho_H$ and $y = \rho_i$, where $i = A, B, C, D, E, F, G, I, O$. The corrected reflectance is then given by:

$$\rho_i(cirrus\ corrected) = \rho_i - (a_i + b_i smooth(\rho_H, 21)) \tag{10}$$

The above method produces remarkable true color and pseudo color images, with the haze from the cirrus cloud scattering much suppressed. The smoothing operator was used with a kernel size of 21 by 21 pixels to reduce the measurement noise in the cirrus channel H.

4.3. Water vapor retrieval

Water vapor retrievals can be obtained using a 3 channel ratio based on the Continuum Interpolated Band Ratio (CIBR) of TOA radiances L_E, L_F and L_G centered around the 940 nm water vapor absorption. The equation used for MTI is (Schlaepfer et al, 1998):

$$CIBR = \frac{\omega_E L_E + \omega_G L_G}{L_f} \tag{11}$$

where $\omega_E = .551$ and $\omega_G = .448$. For bright surfaces ($\rho > 0.2$) the CIBR approximates the total water vapor transmission from the sun to the ground and to the sensor. Over dark surfaces such as water however the radiances L_i are mostly influenced by the path scattering terms which depend on the aerosol loading and in the case of channel F on the amount of water vapor. If we plot the CIBR as a function of the surface reflectance in channel E we find that the CIBR is higher (less water vapor) over dark surfaces than over adjacent brighter surfaces. In Schlaepfer et al, 1998, we introduced the Atmospherically Pre-corrected Differential Absorption (APDA) technique to correct the water vapor over darker surfaces. The technique is quite complicated and involves look-up tables and a lot of fine-tuning to give good results. For MTI we are interested, in particular for the robust SST retrieval, in retrieving the water vapor over water surfaces.

One of the currently studied algorithms tries to estimate water vapor near bodies of water. The assumption is that for a given scene the atmospheric water vapor is spatially relatively smooth and thus across a boundary of water to land should be continuous. The dark/bright APDA we have used has the form:

$$APDA = \frac{\omega_E(L_E - fmin(L_E) + \omega_G L_G - fmin(L_G)}{L_f - fmin(L_F)} \tag{12}$$

where the terms $fmin(L_i)$ are an approximation of the path radiance with the factor f between 0.0 and < 1.0. The algorithm has the following steps:

1. The water mask WM or alternatively a dark mask DM is computed using TOA reflectances in channels C and D.

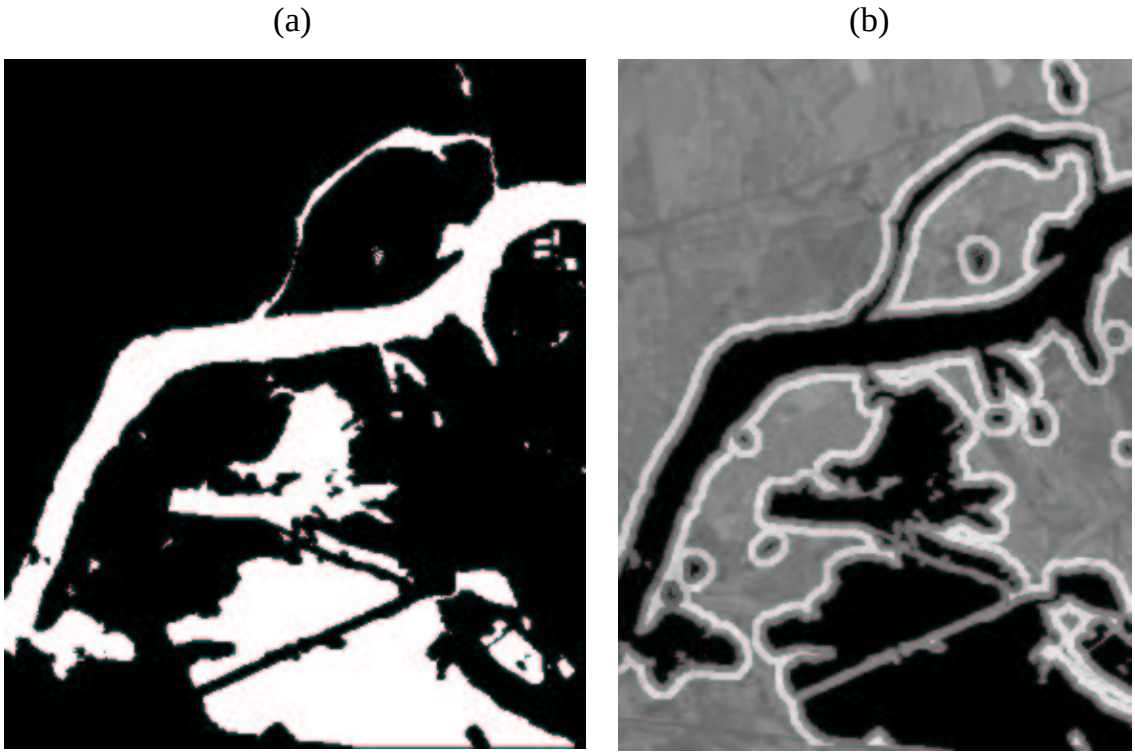

Figure 7. (a) NDVI ρ_C based water mask and (b) "near dark" water pixels in white used for dark/bright based APDA.

2. A "near water" or "near dark" target mask is generated by the logical operation over two dilated versions of the water mask (e.g. using a circular kernel with a diameter of 15 pixels):

$$NMask = DILATE(DILATE(Mask, kernel), kernel) \cap DILATE(Mask, kernel),$$

where $Mask = \{WM,\ DM\}$. See Figure 7 (b) for an example of the "near water" mask.

3. The user specifies a factor f and a point scatter plot of the APDA ratio is plotted versus the reflectance ρ_E for all water or dark area pixels and in another color for all "near water" or "near dark" target pixels.

4. The previous step is repeated until the points of both classes lie visually on a horizontal line. Other measures for good matches are: the means and/or standard deviations are similar.

In Figure 8 we contrast CIBR and APDA ratio images of a sub-scene, where the APDA ratio is very similar near the river as well as inside the river. The algorithm works well for uniform water vapor distributions.

5. Level-2 interactive analysis tool

To test various Level-2 algorithms on AVIRIS derived MTI simulated data sets, we wrote an Interactive Analysis Tool (IAT). As seen in Figure 3 many of the products are intimately connected with each other. Often a mask such as water or dense dark vegetation is needed to automate an algorithm or restrict the locations where an algorithm should be applied. We have built in the following salient features into IAT:

- The program is built of many individual algorithms (some Level-2 products have several choices) each with a set of inputs and outputs.
- While the program is run interactively results are displayed visually and the user can set thresholds etc.

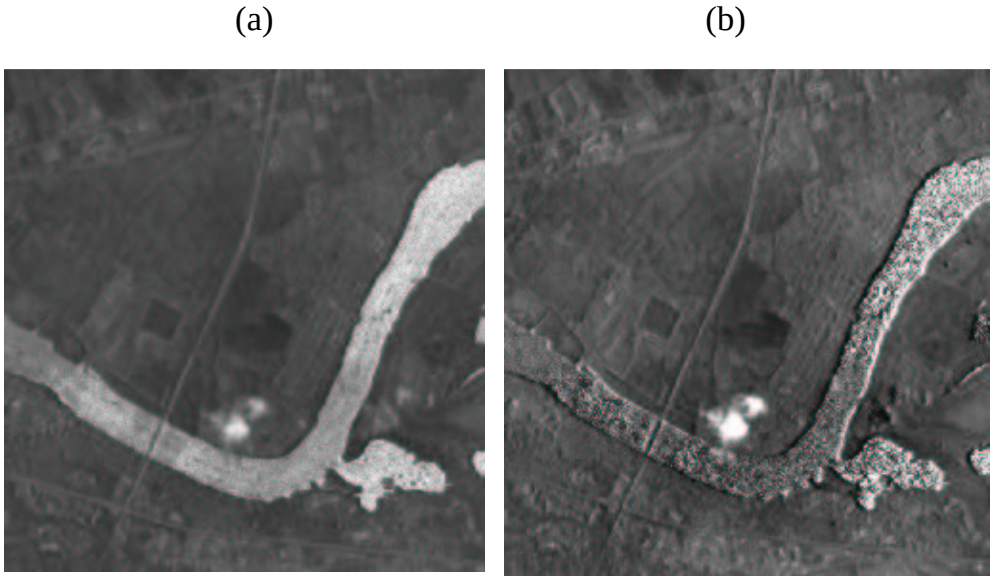

Figure 8. (a) CIBR and (b) dark/bright based APDA for a partial scene with a river (AVIRIS file name f970817t01p02-r06-sc11).

- The user's actions are all stored in a journal file which can later be used to re-play the session or used to process other scenes or provide support in developing or de-bugging complex retrievals.
- The user can select to output images and scene specific settings to a hyper text mark-up language (HTML) file for documentation purposes with included references to GIF and JPEG format images for important results like images, spectra and scatter plots.
- MTI channel and geometry specific interfaces to applications like MODTRAN can aid in the analysis and atmospheric correction.

It is important to note that the interactive tool complements the standard pipeline processing and other commonly used commercial software. To test the Level-2 algorithms we converted over 50 AVIRIS scenes to MTI band averaged TOA radiance data. The scenes contained a variety of different sites in the continental US.

6. Conclusions

MTI has a number of science retrievals which can be used either by themselves or in a processing chain or pipeline. Since some of the products are scene dependent, different paths can be taken through the processing chain. The Level-2 processing system described is flexible enough to allow quick changes and fixes if necessary. The interactive tool described is a complement to existing general purpose software and performs MTI specific tasks with a minimum of user interaction, records the user's action in a journal and creates automatic Web documentation of the process.

7. Acknowledgments

The US Department of Energy supports this work. The spectral and spatial water masks were developed by Steve Alferink, a summer student at LANL. Joseph Winkles, a summer student at LANL implemented a prototype interactive image browsing tool which formed the basis for IAT.

References

Borel, C.C. and S.A.W. Gerstl, "Adjacency-blurring-effect of scenes modeled by the radiosity method," Proc. SPIE'92, Orlando, FL, pp. 620-624, 1992.

Borel, "Nonlinear spectral mixing theory to model multi-spectral signatures," Proc. Eleventh Thematic Conference and Workshops on Applied Geologic Remote Sensing, Las Vegas, NV, pp. II-11 - II-20, 1996a.

Borel, C.C., W.B. Clodius and J. Johnson, "Water vapor retrieval over many surface types," SPIE AeroSense'96, Proc. Vol. 2758, April 1996b.

Borel, C.C., P.V. Villeneuve, W.B. Clodius, J.J. Szymanski and A.B. Davis, "Practical atmospheric correction algorithms for a multispectral sensor from the visible through the thermal spectral region," SPIE conference 3717 on Algorithms for Multispectral and Hyperspectral Imagery, Orlando, 5-9 April, 1999a.

Borel, C.C., W.B. Clodius, J.J. Szymanski and J. Theiler, "Comparing robust and physically based sea surface temperature retrievals for high resolution, multispectral thermal sensors using one or multiple looks," SPIE conference 3717 on Algorithms for Multispectral and Hyperspectral Imagery, Orlando, 5-9 April, 1999b.

Brumby, S.P., J.P. Theiler, J.J. Szymanski, J. Bloch and M. Mitchell, "Investigation of image feature identification by a genetic algorithm," SPIE conference 3812, Denver, 1999.

Garrett, A.J., R.J. Kurzeja, B.L. O'Steen, M.J. Parker, M.M.Pendergast, E. Villa-Aleman, "Post-launch validation of multispectral thermal imager (MTI) data and algorithms,", SPIE conference 3753, Denver, 1999.

Gisler, G. and C.C. Borel, "Neural network identifications of spectral signatures," Proc. Eleventh Thematic Conference and Workshops on Applied Geologic Remote Sensing, Las Vegas, NV, pp. II-21-29, 1996.

Morel, A.,"Optical modeling of the upper ocean in relation to its biogenous matter content (case 1 waters)," Journal of Geophysical Research, Vol.93, No C9, pp 10749-10768, 1988.

Jacquemoud,S., PROSPECT model, *http://cstars.ucdavis.edu/people/stephane/prospect.htm*, 1995.

Jensen, J.R., *Introductory digital image processing - a remote sensing perspective*, Prentice Hall, 2nd edition, 1996.

Kaufman, Y.J., and Tanré, D., "Strategy for direct and indirect methods for correcting the aerosol effect on remote sensing: from AVHRR to EOS- MODIS," Remote Sens. Environ, 55:65-79, 1996.

Kruse, F.A. et al, "The spectral image processing system (SIPS) - interactive visualization and analysis of imaging spectrometer data," RSE Vol. 44, no. 2/3, pp 145-163, 1993.

Schlaepfer, D., C.C. Borel, J. Keller and K.I Itten, "Atmospheric pre-corrected differential absorption technique to retrieve columnar water vapor," RSE Vol. 65, no. 3, pp353-366, 1998.

Smith, B.W. (ed), "Handbook of science algorithms for the multi-spectral thermal imager," Los Alamos unclassified report, LA-UR-98-306, 129 p., 1998.

Szymanski, J.J., C.C. Borel, Q.O. Harberger, P. Smolarkiewicz and J. Theiler, "Subpixel temperature retrieval with multispectral sensors," SPIE conference 3717 on Algorithms for Multispectral and Hyperspectral Imagery, Orlando, 5-9 April, 1999.

Theiler, J. and G. Gisler, "A contiguity-enhanced k-means clustering algorithm for unsupervised multispectral image segmentation," Proceedings of the SPIE - The International Society for Optical Engineering, vol.3159, 108-118, 1997.

Tornow, C. and C. C. Borel, "Multi-angular multi-spectral night-time water temperature retrieval," MTI Technical Report MTI-94-001, 1994a.

Tornow, C., C. C. Borel, and B. J. Powers, "Robust water temperature retrieval using multi-spectral and multi-angular IR measurements," Proc. IGARSS '94, 441-443, 1994.

Vermote, E., 6S code *ftp://kratmos.gsfc.nasa.gov/6S*. 1997.